Hindawi
Journal of Nanomaterials
Volume 2022, Article ID 5186069, 6 pages
https://doi.org/10.1155/2022/5186069

Research Article

Dynamic Beam Switching by the Highly Sensitive Metasurface Composed of All-Metallic Split-Ring Resonators

Wenrong Si,[1] **Chenzhao Fu**,[1] **Fengyuan Gan**,[2] **Dun Lan**,[2] **and Wei Li**[2]

[1]*State Grid Shanghai Electrical Power Research Institute, Shanghai 200437, China*
[2]*State Key Laboratory of Functional Materials for Informatics, Shanghai Institute of Microsystem and Information Technology, CAS, Shanghai 200050, China*

Correspondence should be addressed to Wei Li; waylee@mail.sim.ac.cn

Received 1 May 2022; Revised 9 June 2022; Accepted 21 June 2022; Published 14 July 2022

Academic Editor: Hiwa M. Ahmed

The development of metasurfaces capable of arbitrarily manipulating electromagnetic waves has created new opportunities for various applications. However, most tunable metasurface devices via different modulation techniques exhibit large fabrication difficulties or narrow bandwidths. Here, we use the all-metallic split-ring resonator to design a dynamically tunable metasurface that is highly sensitive to the ambient refractive index and capable of broadband beam switching. Different from the previous optical scatters, the split-ring resonator is put on the metal substrate. Due to the existence of metallic substrate and large interaction of corner modes, the proposed resonator has small ohmic loss and high sensitivity to the ambient refractive index. By arraying the all-metallic split-ring resonators with different parameters, dynamic beam switching of anomalous reflection is demonstrated numerically. In particularly, the designed metasurface exhibits the dynamic beam switching in a broadband wavelength range of $\Delta\lambda \approx 100$ nm. Such an all-metallic metasurface with high sensitivity can greatly reduce the designing difficulty of the tunable optical devices. The dynamic metadevices may find potential applications in stealth camouflage, information encryption, and data storage.

1. Introduction

Metasurfaces are a two-dimensional array structure composed of artificially designed optical scatterers with subwavelength size. Due to the excellent wavefront controlling capability and spatial resolution [1, 2], functional metadevices hold great promise in next-generation wearable devices and thin optical systems for imaging and sensing. They find important applications in the fields of stealth camouflage [3], virtual/augmented reality [4, 5], biosensing [6], and color display [7]. However, because metasurfaces with discontinuous phase distributions are not sensitive to changes in ambient refractive index, most metadevices are static and have a single function. A dynamically tunable metasurface is more flexible and can further expand the application of metasurface functional devices [8–10].

In recent years, some studies have been conducted on developing dynamic metasurface devices via different modulation techniques. For example, the hydrogenation and dehydrogenation reactions of magnesium were utilized to design dynamic metasurface holograms, which could be used for optical information processing and encryption [11, 12]. However, the magnesium hydrogenation and dehydrogenation reactions are time-consuming, and hydrogen is highly combustible and dangerous, which is not suitable for widespread application. By stretching the polydimethylsiloxane substrate to change the lattice constant of the Au nanorod array, a metasurface zoom lens of the continuous focal length change from 150 μm to 250 μm was realized [13]. By utilizing the phase change material, plasmonic metasurfaces for beam switching and bifocal lensing [14] and mid-infrared tunable metasurface capable of broad transmittance spectral shift of 500 nm [15] were successfully demonstrated. However, the metasurfaces in these works are composed of different materials, including elastic material/phase change material and metallic material, which increase the complexity of the structure and the difficulty of fabrication. Based on the nonlinear Kerr effect, a 2D high-Q metalens, which

consisted of Si nanoantennas including the subtle and periodic perturbations, with focal lengths varying from 4 to 6.5 μm was realized [16]. By using the birefringence effect of liquid crystal molecules, dynamic beam switching with an efficiency of 50% is achieved based on the Si nanodisk [17]. However, these two metasurface structures exhibit a narrow-band response due to the resonant effect. Therefore, the realization of broadband and easily manufacturable dynamic metasurface still remains a challenging problem.

In the study, a highly sensitive metasurface is designed based on the all-metallic split-ring resonator, and the dynamically tunable beam switching with a broadband response is demonstrated. Here, the all-metal split-ring resonator can support symmetric and antisymmetric surface plasmon polariton (SPP) modes. Different from the previous optical scatterers placed on dielectric substrates, the powers of two SPP modes are mainly distributed in the external environment (>95%) due to the existence of a metallic substrate and the large interaction of corner modes. As a result, both resonant modes have small ohmic loss and high sensitivity to the ambient refractive index. With the change of the ambient medium from water to a microbubble ($|\Delta n| = 0.333$) by using the laser-induced bubble effect, the shift of reflected spectra of the resonator exceeds 200 nm. Consequently, a dynamic beam switching metasurface is demonstrated numerically by arraying the all-metallic split-ring resonators with different structural parameters. More importantly, the dynamic switching performance exhibits a broadband response (850~950 nm).

2. Principal Analysis

Figure 1(a) shows the proposed unit cell structure, where a split-ring resonator is put on a metallic substrate. Here, the material of the metallic resonator and substrate both are set to gold, and the refractive index of the ambient dielectric of the resonator is $n = 1.333$. The vertical view of the split-ring resonator is shown in the inset in Figure 1(a). The period and width of the resonator are set as $p = 400$ nm and $w = 50$ nm, respectively. The opening angle and radius of the resonator are denoted by α and R, respectively. The all-metallic split-ring resonator can support symmetric and antisymmetric SPP modes [18–20]. At 45° polarized light incidence, the symmetric mode in the all-metallic resonator can be excited. The electric field distribution of the symmetric resonant mode is depicted in Figure 1(b). At 135° polarized light incidence, the antisymmetric mode in the all-metallic resonator is excited. The electric field distribution of the antisymmetric resonant mode is depicted in Figure 1(c). As can be seen from the field distribution, due to the existence of a metallic substrate and the large interaction of corner modes, the evanescent fields of the two SPP modes are mainly distributed in the ambient dielectric (>95%). This value is much greater than that of the metal-dielectric and metal-dielectric-metal unit cell structures (<55%) [21–24]. Therefore, the resonance mode of the all-metal split-ring resonator has small ohmic loss and high sensitivity. When the ambient dielectric changes from water ($n = 1.333$) to a microbubble ($n = 1.0$) via the laser-induced bubble effect [25], the resonant wavelength of the all-metallic resonator shifts significantly (>200 nm).

At y-polarized light incidence, the symmetric and antisymmetric resonant modes in the all-metallic resonator are excited simultaneously according to the vector superposition principle. When the phase difference between the two resonant modes is not equal to $m\pi$ (where m is an integer), the reflected beam of the resonator contains the co-polarized (y-axis) component, as well as the cross-polarized (x-axis) component. By changing the opening angle and radius of the all-metallic split-ring resonator, the amplitude and phase of the reflected beam are efficiently modulated. Also, the phase change of the reflected beam with cross-polarization can cover a broad range from 0 to 2π. Thus, the reflected beam with cross-polarization is primarily focused. At the incident wavelength of $\lambda_0 = 850$ nm, the calculated amplitudes and phases of the reflected beam with cross-polarization of the all-metallic resonator at different opening angles and radii when the ambient refractive indices are $n = 1.333$ and $n = 1.0$ are displayed in Figure 2. The amplitude reflections at the refractive index of the ambient dielectric of $n = 1.333$ are much larger than those at the ambient refractive index of $n = 1.0$ in the range of $120\,\text{nm} < R < 170\,\text{nm}$ and $\alpha < 270°$. The phase change of the all-metallic resonator at the ambient refractive index of $n = 1.333$ can range from 0 to 2π by changing the structural parameters, while the phase change is difficult to cover the range of $0–2\pi$ at the ambient refractive index of $n = 1.0$. The dynamically tunable property is quite different from the metallic nanostructures placed on the dielectric and dielectric-metal film, which exhibits almost the same varying tendency for the amplitudes and phases under different ambient dielectrics [20]. This phenomenon confirms that the all-metallic split-ring resonator is more sensitive to the ambient dielectric than the previous metallic nanostructures. In addition, when the opening angle and radius of the all-metallic resonator are $\alpha = 100°$ and $R = 150$ nm, respectively, the amplitudes of the cross-polarization reflected beam can exceed 0.635 at the ambient refractive index of $n = 1.333$ in the wavelength range from $\lambda_0 = 850$ nm to $\lambda_0 = 950$ nm. The polarization conversion efficiencies can reach up to 90%. In contrast, the amplitude of the cross-polarization reflected beam of the resonator is smaller than 0.041 when the ambient refractive index is $n = 1.0$. Therefore, by arraying all-metallic split-ring resonators with different geometry parameters, dynamic broadband metadevices with different functions can be designed based on the laser-induced bubble effect.

Based on the all-metallic split-ring resonator, we design the highly sensitive all-metallic metasurface and demonstrate broadband dynamic beam switching. The amplitude and phase of the cross-polarization reflected beam are efficiently modulated by changing the opening angle and radius of the all-metallic resonator. In consideration of the reflection efficiencies, the radius of the split-ring resonator is set as $R = 150$ nm. At the refractive index of the ambient dielectric of $n = 1.333$, the phase change of the reflected beam with cross-polarization can still range from 0 to 2π by changing

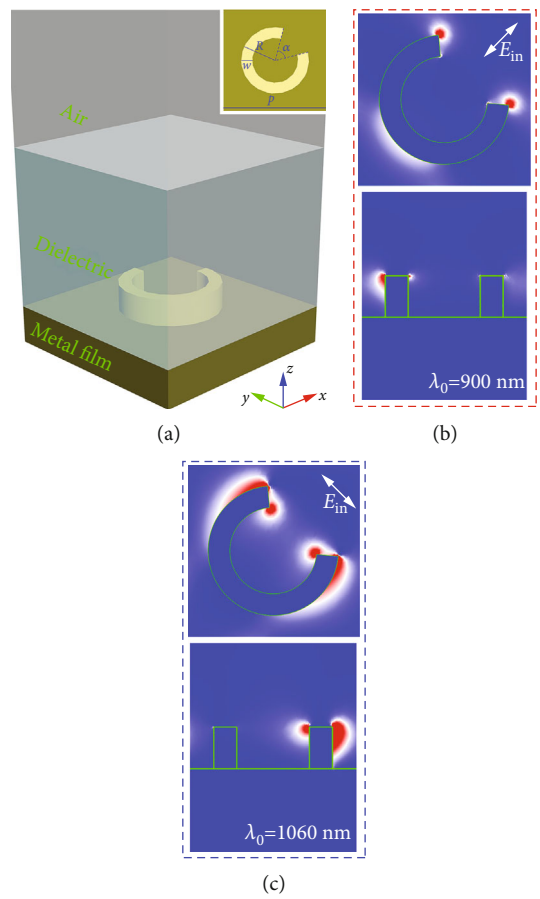

FIGURE 1: Schematic view of the structure of the split-ring resonator and field distribution diagram of the resonant modes: (a) schematic view of the structure; inset: vertical view of the resonator; (b) field distribution diagram of the symmetric resonant mode; and (c) field distribution diagram of the antisymmetric resonant mode.

the opening angle of the resonator, as displayed by the blue dotted line in Figure 3(a). The selected six-unit cells structures are shown in Figure 3(b). The opening angles of the six-unit cells are $\alpha_1 = 33^\circ$, $\alpha_2 = 90^\circ$, $\alpha_3 = 144^\circ$, $\alpha_4 = 195^\circ$, $\alpha_5 = 249^\circ$, and $\alpha_6 = 273^\circ$, respectively. The phase change of the cross-polarization reflected beam of the six-unit cells changed linearly at the ambient refractive index of $n = 1.333$. Comparatively, the phase change is smaller than 0.75π at the ambient refractive index of $n = 1.0$ (the blue solid line in Figure 3(a)). For the amplitude change, the amplitudes of cross-polarization reflected beam are greater than 0.5 at the ambient refractive index of $n = 1.333$ (black dotted line in Figure 3(a)), whereas the amplitudes are smaller than 0.05 at the ambient refractive index of $n = 1.0$ (black solid line in Figure 3(a)). The abovementioned phenomenon also shows that the all-metallic split-ring resonator is highly sensitive to changes in the ambient refractive index.

3. Design and Results

By arranging the six-unit cell structures in a sequence, the gradient metasurface is formed, as displayed in Figure 4(a). When the y-polarized light is incident on the metasurface, the reflected beam includes the normal reflected beam (co-polarization) and anomalous reflected beam (cross-polarization). For anomalous reflected beam, the phase gradient of the metasurface interface is $d\varphi/dx = \pi/1.2\,\text{rad}/\mu\text{m}$. The reflection angle of the anomalous reflected beam can be calculated according to the following equation:

$$\theta_r = \arcsin\left(\frac{\lambda_0}{2\pi n}\frac{d\varphi}{dx} + \sin\theta_i\right), \quad (1)$$

where θ_i and θ_r represent the incident angle and anomalous reflection angle of the beam, respectively, and n represents the refractive index of the ambient dielectric. By using the finite element method, the optical performance of the gradient metasurface is studied in detail. Under the incident wavelength of $\lambda_0 = 850\,\text{nm}$ and dielectric refractive index of $n = 1.333$, anomalous reflection angle of the metasurface at different incident angles is displayed in Figure 4(b). It can be observed that in the range of $\theta_i = -20^\circ$ to 30°, the anomalous reflection angles obtained by the simulation (black dots in Figure 4(b)) agree well with the calculated results by using Equation (1) (red line in Figure 4(b)). Therefore, the gradient metasurface of anomalous reflection is demonstrated in a wide range of incident angles. At $\theta_i = -$

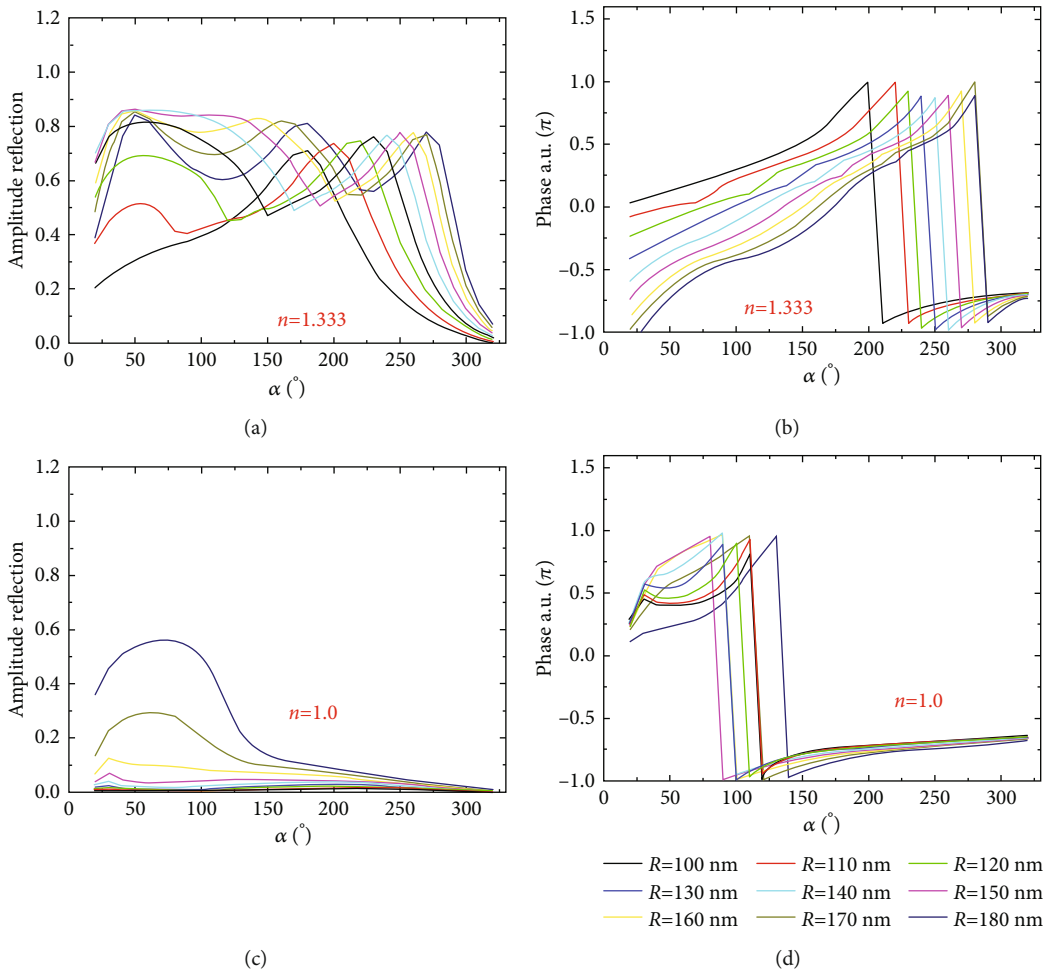

Figure 2: Amplitudes and phases of the cross-polarization reflected beam at different structural parameters: (a) amplitudes and (b) phases at the refractive index of the ambient dielectric of $n = 1.333$ and (c) amplitudes and (d) phases at the refractive index of the ambient dielectric of $n = 1.0$.

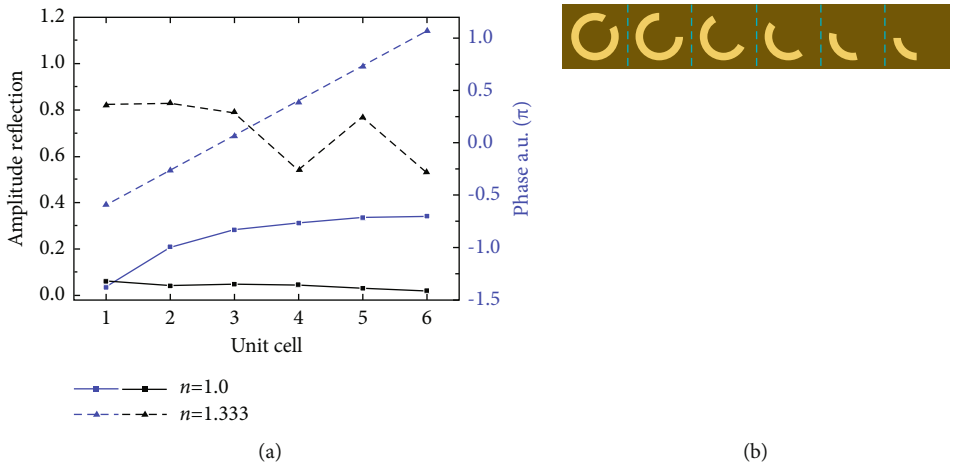

Figure 3: Amplitude and phase changes of the cross-polarization reflected beam of the split-ring resonator under different ambient dielectrics: (a) amplitude and phase change of the six-unit cells and (b) schematic view of the six-unit cells structures.

30°, the simulated anomalous reflection angle is different from the calculated angle, which is attributed to the nonlinear phase change of the six-unit cells at large incident angle. By adding a large field of view phase compensation factor, the field of view of the designed gradient metasurfaces can be further increased.

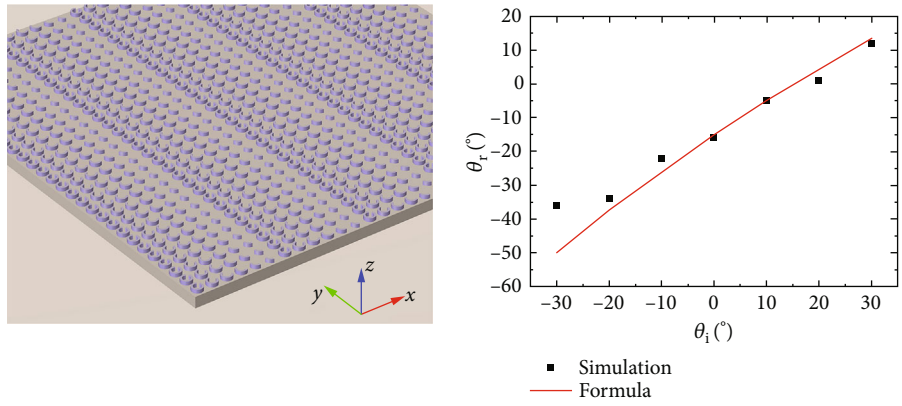

Figure 4: Designed dynamic metasurface and anomalous reflection phenomenon of the metasurface: (a) schematic view of the designed metasurface structure and (b) anomalous reflection angles of the metasurface at different incident angles.

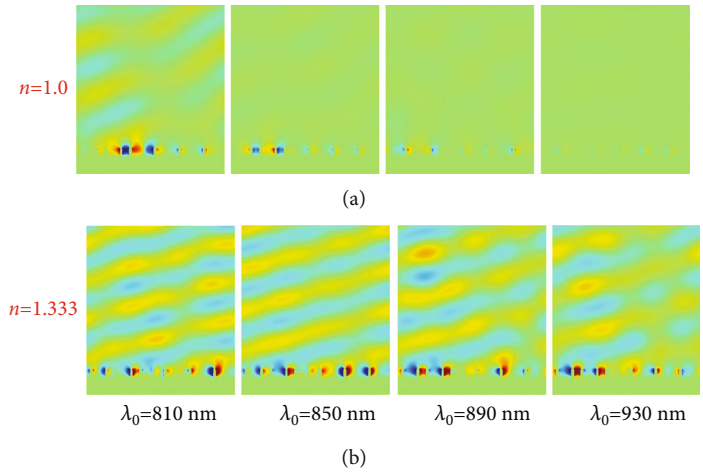

Figure 5: Simulation results: (a) scattering field distributions (E_x) at different incident wavelengths when the ambient refractive index is $n = 1.0$ and (b) scattering field distributions (E_x) at different incident wavelengths when the ambient refractive index is $n = 1.333$.

For the incident angle of $\theta_i = 0°$, the scattering field distributions (E_x) of the metasurface at different wavelengths are shown in Figure 5. When the ambient refractive index is $n = 1.0$, the powers of cross-polarization reflected beam of the metasurface are relatively small at the wavelength of $\lambda_0 \geq 850$ nm, which is consistent with the above analysis and calculation results. In contrast, at the refractive index of the ambient dielectric of $n = 1.333$, the anomalous reflections of the cross-polarization beam are observed clearly because of the large reflection amplitude of the cross-polarization component of the resonators. Consequently, the dynamic beam switching metasurface is successfully demonstrated by changing the refractive index of the ambient dielectric. From our previous work, the ambient dielectric of the metasurface could be dynamically modulated between water ($n = 1.333$) and a microbubble ($n = 1.0$) based on the laser-induced bubble effect [25]. Moreover, the dynamic switching properties exhibit a broadband response ($\lambda_0 = 850 \sim 950$ nm), which is greater than that of dielectric metasurfaces in previous work [16, 17]. It should be noted that the anomalous reflections of the all-metallic metasurface exhibit uneven intensity distributions when the working wavelength deviating from the optimized wavelength. By using particle swarm algorithms, the all-metallic metasurface can be optimized further at multiple working wavelengths to obtain even intensity distributions. Such a dynamic metasurface device with high sensitivity may find potential applications, such as stealth camouflage, information encryption, and data storage. By utilizing the far-field optical microscopy detection system, the beam deflection of the designed dynamic metalens can be investigated experimentally.

4. Conclusion

In summary, by arraying the all-metallic split-ring resonator with different geometry parameters, the highly sensitive gradient metasurface was designed, and dynamic beam switching was demonstrated. Here, the proposed metallic split-ring resonator could support the symmetric and antisymmetric SPP modes. Due to the existence of metallic substrate and

large interaction of corner modes, the two SPP modes exhibited lower ohmic loss and higher sensitivity than the previous optical scatterers placed on the dielectric substrate. At the refractive index of the ambient dielectric of $n = 1.333$, the amplitudes of the reflected beam with cross-polarization of the all-metallic resonator were much larger than that at the ambient refractive index of $n = 1.0$ in the range of $120\,\text{nm} < R < 170\,\text{nm}$ and $\alpha < 270^\circ$. Moreover, the phase change of the reflected beam with cross-polarization could range from 0 to 2π at the ambient refractive index of $n = 1.333$ by changing the structural parameters of the resonator. Therefore, a dynamic beam switching metasurface with a broadband response ($\Delta\lambda \approx 100\,\text{nm}$) was realized numerically by arraying the resonators with different geometry parameters. The proposed all-metallic metasurface with high sensitivity can greatly reduce the designing difficulty of the tunable optical devices. In the future, various dynamic metadevices, such as beam shapers, metasurface hologram, and planar lenses, could be designed based on the all-metallic split-ring resonators with excellent properties. These dynamic metadevices might find potential applications in stealth camouflage, information encryption, and data storage.

Data Availability

The data used to support the findings of this study are included within the article.

Conflicts of Interest

The authors declare that there is no conflict of interest regarding the publication of this paper.

Acknowledgments

This work was supported by Science and Technology Project from State Grid Shanghai Electric Power Company of No. 52094020005J.

References

[1] N. F. Yu and F. Capasso, "Flat optics with designer metasurfaces," *Nature Materials*, vol. 13, no. 2, pp. 139–150, 2014.

[2] M. Khorasaninejad, W. T. Chen, R. C. Devlin, J. Oh, A. Y. Zhu, and F. Capasso, "Metalenses at visible wavelengths: diffraction-limited focusing and subwavelength resolution imaging," *Science*, vol. 352, no. 6290, pp. 1190–1194, 2016.

[3] X. J. Ni, Z. J. Wong, M. Mrejen, Y. Wang, and X. Zhang, "An ultrathin invisibility skin cloak for visible light," *Science*, vol. 349, no. 6254, pp. 1310–1314, 2015.

[4] G. Y. Lee, J. Y. Hong, S. H. Hwang et al., "Metasurface eyepiece for augmented reality," *Nature Communications*, vol. 9, no. 1, p. 4562, 2018.

[5] Z. Y. Li, P. Lin, Y. W. Huang et al., "Meta-optics achieves RGB-achromatic focusing for virtual reality," *Science Advances*, vol. 7, no. 5, 2021.

[6] D. Rodrigo, O. Limaj, D. Janner et al., "Mid-infrared plasmonic biosensing with graphene," *Science*, vol. 349, no. 6244, pp. 165–168, 2015.

[7] W. J. Joo, J. Kyoung, M. Esfandyarpour et al., "Metasurface-driven OLED displays beyond 10, 000 pixels per inch," *Science*, vol. 370, no. 6515, pp. 459–463, 2020.

[8] H. Gao, X. Fan, W. Xiong, and M. Hong, "Recent advances in optical dynamic meta-holography," *Opto-Electronic Advances*, vol. 4, no. 11, article 210030, 2021.

[9] C. Meng, P. C. V. Thrane, F. Ding et al., "Dynamic piezoelectric MEMS-based optical metasurfaces," *Science Advances*, vol. 7, no. 26, 2021.

[10] X. G. Zhang, W. X. Jiang, H. L. Jiang et al., "An optically driven digital metasurface for programming electromagnetic functions," *Nature Electronics*, vol. 3, no. 3, pp. 165–171, 2020.

[11] J. X. Li, S. Kamin, G. Zheng, F. Neubrech, S. Zhang, and N. Liu, "Addressable metasurfaces for dynamic holography and optical information encryption," *Science Advances*, vol. 4, no. 6, article eaar6768, 2018.

[12] P. Yu, J. Li, S. Zhang et al., "Dynamic janus metasurfaces in the visible spectral region," *Nano Letters*, vol. 18, no. 7, pp. 4584–4589, 2018.

[13] H. S. Ee and R. Agarwal, "Tunable metasurface and flat optical zoom lens on a stretchable substrate," *Nano Letters*, vol. 16, no. 4, pp. 2818–2823, 2016.

[14] X. H. Yin, T. Steinle, L. Huang et al., "Beam switching and bifocal zoom lensing using active plasmonic metasurfaces," *Light: Science & Applications*, vol. 6, no. 7, article e17016, 2017.

[15] W. L. Dong, Y. Qiu, X. Zhou et al., "Tunable mid-infrared phase-change metasurface," *Advanced Optical Materials*, vol. 6, no. 14, article 1701346, 2018.

[16] E. Klopfer, M. Lawrence, D. R. Barton, J. Dixon, and J. A. Dionne, "Dynamic focusing with high-quality-factor metalenses," *Nano Letters*, vol. 20, no. 7, pp. 5127–5132, 2020.

[17] A. Komar, R. Paniagua-Domínguez, A. Miroshnichenko et al., "Dynamic beam switching by liquid crystal tunable dielectric metasurfaces," *ACS Photonics*, vol. 5, no. 5, pp. 1742–1748, 2018.

[18] L. X. Liu, X. Zhang, M. Kenney et al., "Broadband metasurfaces with simultaneous control of phase and amplitude," *Advanced Materials*, vol. 26, no. 29, pp. 5031–5036, 2014.

[19] X. Q. Zhang, Z. Tian, W. Yue et al., "Broadband terahertz wave deflection based on C-shape complex metamaterials with phase discontinuities," *Advanced Materials*, vol. 25, no. 33, pp. 4567–4572, 2013.

[20] F. Y. Gan, X. Yang, Y. Zhou, and W. Li, "Wavelength-multiplexed varifocal and switchable metalens with all-metallic C-shaped antennas," *Optics and Laser Technology*, vol. 147, p. 107630, 2022.

[21] N. F. Yu, F. Aieta, P. Genevet, M. A. Kats, Z. Gaburro, and F. Capasso, "A broadband, background-free quarter-wave plate based on plasmonic metasurfaces," *Nano Letters*, vol. 12, no. 12, pp. 6328–6333, 2012.

[22] P. C. Wu, W. Y. Tsai, W. T. Chen et al., "Versatile polarization generation with an aluminum plasmonic metasurface," *Nano Letters*, vol. 17, no. 1, pp. 445–452, 2017.

[23] F. Ding, Z. Wang, S. He, V. M. Shalaev, and A. V. Kildishev, "Broadband high-efficiency half-wave plate: a supercell-based plasmonic metasurface approach," *ACS Nano*, vol. 9, no. 4, pp. 4111–4119, 2015.

[24] G. X. Zheng, H. Mühlenbernd, M. Kenney, G. Li, T. Zentgraf, and S. Zhang, "Metasurface holograms reaching 80% efficiency," *Nature Nanotechnology*, vol. 10, no. 4, pp. 308–312, 2015.

[25] F. Y. Gan, Y. Wang, C. Sun et al., "Widely tuning surface plasmon polaritons with laser-induced bubbles," *Advanced Optical Materials*, vol. 5, no. 4, article 1600545, 2017.